# Supporting Information for "Empirically estimated electron lifetimes in the Earth's radiation belts: 1. Observations"

S. G. Claudepierre[1,2], Q. Ma[2,3], J. Bortnik[2], T. P. O'Brien[1], J. F. Fennell[1], and J. B. Blake[1]

[1]Space Sciences Department, The Aerospace Corporation, El Segundo, California, USA

[2]Department of Atmospheric and Oceanic Sciences, UCLA, Los Angeles, California, USA

[3]Center for Space Physics, Boston University, Boston, Massachusetts, USA

## Contents of this file

1. Text S1 to S2
2. Figures S1 to S2
3. Table S1

## Additional Supporting Information (Files uploaded separately)

1. Datasets S1 to S6

## Introduction

The following information is provided in support of the main manuscript. We provide data files that contain the statistical database of lifetimes obtained as described in the main manuscript. We also provide further details on the empirical lifetime estimates from

prior published works that are used in the main manuscript, including the spacecraft, orbit, and instrumentation, with all acronyms spelled out. Finally, we provide additional details regarding the automated algorithm that is used to obtain the empirical lifetime database.

**Text S1.**

Table S1 lists the details on the empirical lifetime estimates from prior published works that are used in the main manuscript. The following sources have been used, with all of the orbital parameters obtained from the NASA Space Science Data Coordinated Archive (https://nssdc.gsfc.nasa.gov):

Vampola (1971) used measurements from the Magnetic Electron Spectrometer (MES) instrument on Orbiting Vehicle 3, number 3 (OV3-3). OV3-3 operated in a Highly Eccentric Orbit (HEO) with launch parameters of 358 km, 4479 km, 81.47° (perigee, apogee, and inclination, respectively).

West, Buck, and Davidson (1981) used measurements from the Electron and Proton Spectrometer (EPS) instrument on Orbiting Geophysical Observatories, number 5 (OGO5). OGO5 operated in a HEO orbit with launch parameters of 272 km x 23 $R_E$, 31.1° (perigee, apogee, and inclination, respectively).

Albert (2000), Seki, Miyoshi, Summers, and Meredith (2005), and Meredith et al. (2006) all used measurements from the Medium Electron Sensor A (MEA) instrument on the

Combined Release and Radiation Effects Satellite (CRRES). CRRES operated in a Geostationary Transfer Orbit (GTO) orbit with launch parameters of 350 km x 5.3 $R_E$, 18.2° (perigee, apogee, and inclination, respectively).

Meredith et al. (2009) used measurements from the Proton/Electron Telescope (PET) instrument on the Solar Anomalous and Magnetospheric Particle Explorer (SAMPEX). SAMPEX operated in a Low Earth Orbit (LEO) with launch parameters of 512 km x 687 km, 81.7° (perigee, apogee, and inclination, respectively).

Benck, Mazzino, Cyamukungu, Cabrera, and Pierrard (2010) used measurements from both the Influence of Space Radiation on Advanced Components (ICARE) instrument on the Satelite de Aplicaciones Cientifico-C (SAC-C), and from the Instrument for Particle Detection (IDP) instrument on the Detection of Electro-Magnetic Emissions Transmitted from Earthquake Regions (DEMETER) satellite. SAC-C operated in a LEO orbit with launch parameters of 700 km x 700 km, 98.2° (perigee, apogee, and inclination, respectively). DEMETER operated in a LEO orbit with launch parameters of 710 km x 710 km, 98° (perigee, apogee, and inclination, respectively).

Su et al. (2012) used measurements from the SC3 instrument on the Spacecraft Charging At High Altitudes (SCATHA) satellite. SCATHA operated in a HEO orbit with launch parameters of 5.3 x 7.8 $R_E$, 7.7° (perigee, apogee, and inclination, respectively).

**Text S2.**

We now provide additional information on the automated algorithm that has been developed to identify exponential decays and calculate the e-folding times of the decays from the MagEIS electron measurements. This algorithm is based on the technique of Benck et al. (2010), which was in turn adapted from that of Meredith et al. (2006), but has been tailored somewhat to accommodate the unique features of the MagEIS data set. Our algorithm begins by considering a time series of electron flux in a fixed $L$ and energy bin, which we denote ($L$,$E$). A smoothed version of the time series is separately calculated first to identify time intervals during which the smoothed flux is decreasing over some minimum time window length. This length is nominally 5 days, but larger values are used in some ($L$,$E$)-bins to obtain better fits and statistics - see below. We refer to the time interval over which the smoothed flux is decreasing as $T$, noting that it is at least 5 days long and can be longer if the smoothed flux is decreasing over a longer time scale. The length of the smoothing window is predetermined and varies in each ($L$,$E$)-bin, though it is nominally in the 1 (no smoothing) to 4 day range. Longer minimum time window lengths and longer smoothing windows are generally used in the inner zone, where the fluxes are less dynamic and more subject to fluctuations related to low counts (Poisson noise) and/or orbital effects. Data gaps in the smoothed time series shorter than 3 days are linearly interpolated across.

Once such an interval, $T$, has been identified, the original (non-smoothed) time series is analyzed and the smoothed time series is no longer used. The flux time series is fit

with an exponential function, $J(t) = J_0 \exp(-t/\tau)$, over $T$. In order to construct a fit, we require that 90% of the flux values in $T$ be non-zero and valid (e.g., non-fill value); there is no interpolation done on the original (non-smoothed) time series. Two goodness-of-fit parameters relating the fit to the flux are recorded, the linear correlation coefficient and the percent error, which is defined as the median symmetric accuracy (Morley, Brito, and Welling (2018)). If the linear correlation coefficient, $r$, is greater than some predetermined threshold and the percent error is less than 25%, then the fit is accepted. As with the smoothing window and minimum time window lengths, the specific $r$-value for each ($L$,$E$)-bin is predetermined, with larger values ($\geq 0.94$) used at higher $L$ and $r \geq 0.8$ almost everywhere (see below). We note, however, that the percent error threshold is fixed at 25% for all ($L$,$E$)-bins. For all subintervals of $T$ that satisfy the minimum time window length requirement for the specific ($L$,$E$)-bin and the 90% requirement for valid flux values, additional exponential fits are obtained as described above. From all of the accepted fits within $T$, the fit with the largest $r$-value is retained as the single fit for the time interval $T$. The above process is then repeated on the next time interval over which the smoothed flux is decreasing, and so on. We emphasize that the smoothed time series is only used to identify time intervals during which the fluxes are decreasing; the exponential fits and statistical database are constructed using the original, daily-averaged flux time series. The entire process is then repeated in each ($L$,$E$)-bin to obtain a statistical database of decay intervals and decay timescales as a function of $L$ and energy.

Figure S1 provides an example of the application of the automated procedure in four $L$ bins and in the fixed energy bin of 467 keV. The daily averaged fluxes are shown in the middle (color) panel across the entire $L$ and time range considered here, 01 Apr 2013 to 01 Apr 2018. The four line plot panels show flux profiles at the four indicated $L$ values. We see that the fluxes in the inner zone decay over long time scales ($\tau > 100$ d), while much more rapid decays are observed in the slot and outer zone ($\tau \sim 1 - 5$ d). The data gap at $L > 3$ early in the time interval is due to the operation of the MagEIS instrument in a mode that does not allow for background corrected data to be produced (see Claudepierre et al., 2015). While it may be tempting to use uncorrected data in such instances, we demonstrate in the main manuscript that background contamination can have a significant impact on lifetime calculations and lead to erroneous results.

As noted in the main manuscript, there are three primary parameters used in the algorithm to identify and accept exponential fits as valid. The first is the number of days used to smooth the daily-averaged flux time series, $N_{smooth}$. This parameter is shown in panel (a) Figure S2 and is used only to search for intervals when the flux is generally decreasing. Above $L$ of 2.5, this parameter is generally in the 1-4 day range, but longer smoothing windows are used in the inner zone. This is because in the inner zone the daily-averaged fluxes are more sensitive to the orbital motion of the Van Allen Probes and its phasing with respect the geomagnetic equator (where a roughly 3 day periodicity is noted). Also, the decay timescales are much longer in the inner zone than elsewhere, so that smoothing over a longer time window helps identify longer time intervals from which the exponential

fits are obtained.

Panel (b) in Figure S2 shows the minimum number of days required for a valid fit, $N_{fit}$, in each energy and $L$ bin. Again, because the lifetimes in the inner zone are generally longer, we require this parameter to be longer than elsewhere to provide a more accurate estimate of the decay timescale. Finally, panel (c) shows the threshold (minimum) linear correlation coefficient used to accept a fit as valid, $r_{thresh}$. This value is reduced in the inner zone below a nominal value of 0.9 used elsewhere so that more decay intervals can be identified. Because of the long decay timescales and the relative paucity of injections into the inner zone at higher energies, there are few events that satisfy the stringent criteria used in the outer slot and outer zone. In general, the criteria on the quality of the fits must be relaxed in the inner zone and at the highest energies to boost statistics.

It is worth noting that the automated algorithm described here is tailored to identify decay intervals on differential fluxes; it will not accurately compute the decay rates during a time interval that contains a two-stage decay in differential flux. This is because the algorithm will identify such an interval as a single decay interval and calculate the decay rate from whichever portion of the decay best satisfies the goodness-of-fit criteria. For a given decay interval this could, in principle, be either the rapid initial decay, or the slower more gradual decay that follows, so that any statistical database obtained would thus contain a mixture of both timescales present in two-stage decays. It is for these reasons that we do not compute electron lifetimes from integral fluxes in this work, nor

compare such estimates with those obtained from other observational studies. A different algorithm than the one described here would be required to properly analyze decays in integral flux measurements.

**Data Set S1.** The file "lifetime_database_tau_mean.txt" contains the mean lifetimes as presented in the main manuscript. The file contains header lines that describe the contents of the comma-separated values in the file.

**Data Set S2.** The file "lifetime_database_tau_median.txt" contains the median lifetimes as calculated in the main manuscript. The file contains header lines that describe the contents of the comma-separated values in the file.

**Data Set S3.** The file "lifetime_database_tau_max.txt" contains the maximum lifetimes as calculated in the main manuscript. The file contains header lines that describe the contents of the comma-separated values in the file.

**Data Set S4.** The file "lifetime_database_tau_min.txt" contains the minimum lifetimes as calculated in the main manuscript. The file contains header lines that describe the contents of the comma-separated values in the file.

**Data Set S5.** The file "lifetime_database_tau_std.txt" contains the standard deviation of the mean lifetimes as presented in the main manuscript. The file contains header lines

that describe the contents of the comma-separated values in the file.

**Data Set S6.** The file "lifetime_database_tau_n.txt" contains the number of decay events as presented in the main manuscript. The file contains header lines that describe the contents of the comma-separated values in the file.

## References

Albert, J. M. (2000, Jan). Pitch Angle Diffusion as Seen by CRRES. *Adv. Space Res.*, *25*(12), 2343-2346. doi: 10.1016/S0273-1177(99)00520-7

Benck, S., Mazzino, L., Cyamukungu, M., Cabrera, J., & Pierrard, V. (2010, Mar). Low altitude energetic electron lifetimes after enhanced magnetic activity as deduced from SAC-C and DEMETER data. *Ann. Geophys.*, *28*(3), 849-859. doi: 10.5194/angeo-28-849-2010

Claudepierre, S. G., O'Brien, T. P., Blake, J. B., Fennell, J. F., Roeder, J. L., Clemmons, J. H., ... Larsen, B. A. (2015, July). A background correction algorithm for Van Allen Probes MagEIS electron flux measurements. *J. Geophys. Res.*, *120*, 5703-5727. doi: 10.1002/2015JA021171

Meredith, N. P., Horne, R. B., Glauert, S. A., Baker, D. N., Kanekal, S. G., & Albert, J. M. (2009, Mar). Relativistic electron loss timescales in the slot region. *J. Geophys. Res.*, *114*(A3), A03222. doi: 10.1029/2008JA013889

Meredith, N. P., Horne, R. B., Glauert, S. A., Thorne, R. M., Summers, D., Albert, J. M., & Anderson, R. R. (2006, May). Energetic outer zone electron loss timescales

during low geomagnetic activity. *J. Geophys. Res.*, *111*(A5), A05212. doi: 10.1029/2005JA011516

Morley, S. K., Brito, T. V., & Welling, D. T. (2018, January). Measures of Model Performance Based On the Log Accuracy Ratio. *Space Weather*, *16*, 69-88. doi: 10.1002/2017SW001669

Seki, K., Miyoshi, Y., Summers, D., & Meredith, N. P. (2005, Feb). Comparative study of outer-zone relativistic electrons observed by Akebono and CRRES. *J. Geophys. Res.*, *110*(A2), A02203. doi: 10.1029/2004JA010655

Su, Y.-J., Johnston, W. R., Albert, J. M., Ginet, G. P., Starks, M. J., & Roth, C. J. (2012, Aug). SCATHA measurements of electron decay times at $5 < L \leq 8$. *J. Geophys. Res.*, *117*(A8), A08212. doi: 10.1029/2012JA017685

Vampola, A. L. (1971). Natural variations in the geomagnetically trapped electron population. In E. A. Warman (Ed.), *Proceedings of the National Symposium on Natural and Manmade Radiation in Space* (p. 539-547).

West, J., H. I., Buck, R. M., & Davidson, G. T. (1981, Apr). The dynamics of energetic electrons in the earth's outer radiation belt during 1968 as observed by the Lawrence Livermore National Laboratory's spectrometer on Ogo 5. *J. Geophys. Res.*, *86*(A4), 2111-2142. doi: 10.1029/JA086iA04p02111

**Table S1.** Previous Empirical Estimates of Electron Decay Timescales

| Reference | Spacecraft/Instrument | Orbit | Energy Channels[a] |
|---|---|---|---|
| Vampola (1971) | OV3-3/MES | HEO | 475 & 957 keV |
| West et al. (1981) | OGO5/EPS | HEO | 266 & 478 keV |
| Albert (2000) | CRRES/MEA | GTO | 510 keV |
| Seki et al. (2005) | CRRES/MEA | GTO | 976 & 1582 keV |
| Meredith et al. (2006) | CRRES/MEA | GTO | 214-1090 keV (8 bins) |
| Meredith et al. (2009) | SAMPEX/PET | LEO | 2-6 MeV (1 bin) |
| Benck et al. (2010) | SAC-C/ICARE & DEMETER/IDP | LEO | 160-1360 keV (13 bins) |
| Su et al. (2012) | SCATHA/SC3 | HEO | 57-289 keV (12 bins) |

[a]Available for the comparisons; not necessarily representative of the full energy range of the instrument.

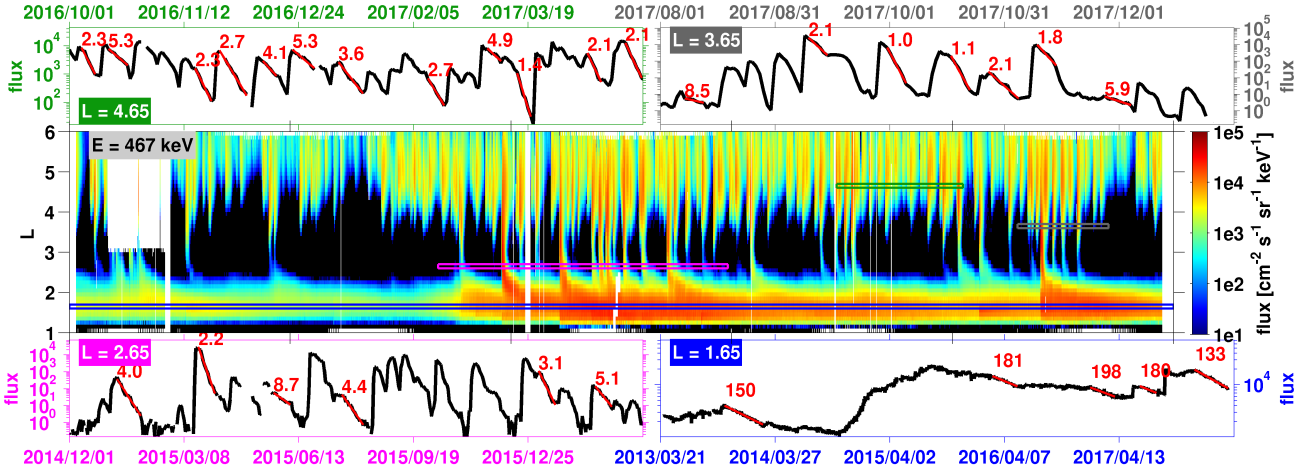


**Figure S1.** Daily-averaged, differential flux for 467 keV electrons averaged over equatorial pitch angles between 70° and 110°. The middle (color) panel shows the fluxes in $L$-versus-time format over the time interval 01 Apr 2013 to 01 Apr 2018. The four line plot panels show flux profiles at the four indicated $L$ values; the time and $L$ regions displayed are highlighted by colored boxes in the middle panel. Exponential decays identified by the automated algorithm are highlighted in red with the calculated decay (e-folding) times indicated, in days.

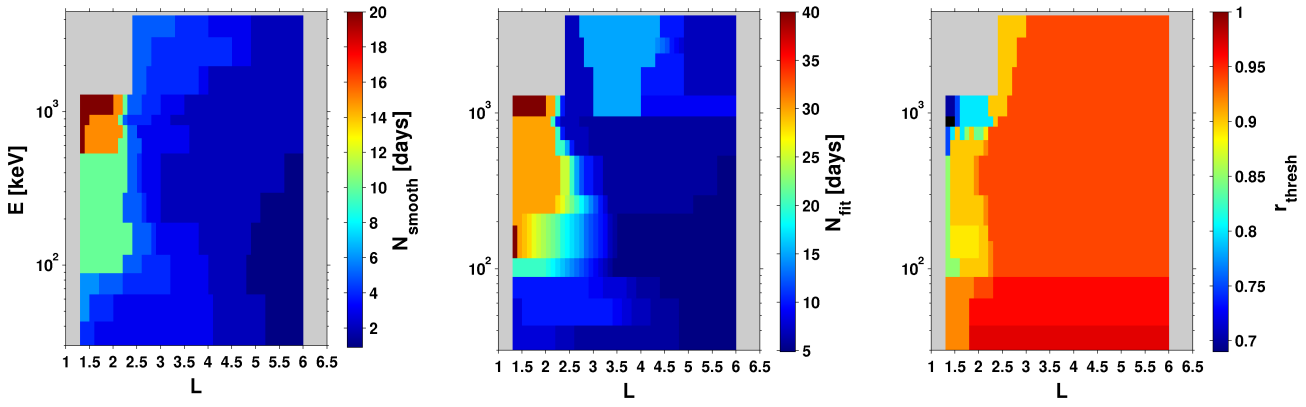


**Figure S2.** Overview of the three parameters used in the automated algorithm in each energy and $L$ bin. **(a)** The number of days used to smooth the time series. **(b)** The minimum number of days required for a valid fit. **(c)** The threshold linear correlation coefficient used to accept a fit as valid.